The Journal of the Astronautical Sciences, Vol. 34, No. 4, October-December 1986 pp. 403–419

Approximate Free-Molecular Flow Torques on Spinning Satellites

Jozef C. Van der Ha[1]

Abstract

General expressions for torques induced by the free-molecular flow interaction with a spinning satellite are presented. Since the results are intended for application to spinning satellites in geostationary transfer orbits a number of simplifications which are consistent with this environment are introduced. Expressions for the torques are obtained by first integrating the contribution of an infinitesimal surface element over the appropriate part of one spin revolution. Afterwards, the expressions are completed by performing the integration over all exposed satellite surface elements. In particular, results are given for idealized cylindrical and box-like satellite configurations.

Introduction

The nature of free-molecular momentum interactions with satellite surfaces has been investigated by many authors over the past few decades. The generally adopted formulation makes use of accommodation coefficients for the normal and tangential momentum transfer, *e.g.*, Schaaf *et al.* [1]. The objective of the early research in this area was related to the calculation of drag coefficients required for predicting orbital decay rates, cf. Cook [2] and Izakov [3].

More recently, elaborate models for prediction of free-molecular forces as well as moments on spacecraft have been constructed and subjected to experimental verification, cf. Boettcher *et al.* [4], [5] and Koppenwallner [6]. Realistic satellite configurations with surface irregularities can be analysed by a numerical superposition of the contributions of a large number of small elementary surface elements.

In the present paper relatively simple closed-form expressions will be derived for free-molecular torques upon extended spinning satellite surfaces. The accommodation coefficients, which are usually not precisely known, appear as parameters in these results allowing sufficient flexibility for performing parametric analyses. Since the

[1]Senior Analyst, European Space Operations Centre (ESA), Robert-Bosch-Str. 5, 6100 Darmstadt, FRG.

application of this work is primarily directed to satellites in geostationary transfer orbits a few minor simplifications are introduced which are compatible with this environment.

The objectives of the investigation are twofold: first, the resulting torque expressions would allow a quick assessment of possible attitude variations of a spinning satellite, for example when crossing the perigee region in a geostationary transfer orbit [7]. Second, the results can be used as building blocks in the precise numerical analyses of highly irregular satellite configurations at substantial savings in computer time as compared to approaches based on infinitesimal elements.

General Model of Aerodynamic Interaction with Satellite Surface

A proper model for aerodynamic interactions with satellite surfaces should be based on free-molecular gas flow theory, as the mean free path of atmospheric particles is large compared to a representative spacecraft dimension for present-day satellite applications. For a typical ARIANE geostationary transfer orbit with perigee altitude near 200 km, a mean free path of about 220 m is found for molecular nitrogen (Boettcher [4]). The re-emission of particles from the satellite's surface results in an increased density near the surface. In this region the mean free path can be shown to be shorter than the undisturbed path by a factor v_w/v, where v is the orbital velocity and v_w is the most probable speed of molecules reflected (Cook [2]). The molecular speed v_w is directly proportional to the square root of the satellite's surface temperature T_w. On the basis of a surface temperature T_w of about 300 °K and a velocity of 10.2 km/s (at perigee) a smallest value for the mean free path of 10 m is obtained. Therefore, one is justified to apply free-molecular flow theory for studying aerodynamic drag effects on a typical satellite in geostationary transfer orbits.

General Model for Pressure and Shear Forces

A commonly adopted model for the pressure and shear forces acting on a surface element due to free-molecular flow makes use of the coefficients for normal and tangential momentum accommodation (Schaaf *et al* [1])

$$\sigma_n = (p_i - p_r)/(p_i - p_w) \tag{1}$$

$$\sigma_t = (\tau_i - \tau_r)/\tau_i \tag{2}$$

where σ_n and σ_t are the normal and tangential momentum accommodation coefficients, p_i and p_r are the normal components of incident and reflected molecular momentum flux, and p_w is the normal momentum component for molecules re-emitted from the surface at Maxwell thermal speed corresponding to T_w. τ_i and τ_r are the tangential components of incident and reflected molecular momentum flux.

Since the re-emission profile of the accommodated molecules at surface temperature may be taken as symmetrically diffuse, re-emission will not induce any shear stresses on the surface. The coefficients defined in equations (1) and (2) are not known a priori and would have to be determined experimentally (*e.g.*, by molecular-beam methods). On the basis of such experiments it has been suggested that for satellite applications σ_n is close to 1 and σ_t is about 0.9 (Izakov [3]). This implies that p_r is virtually equal to p_w, meaning that the incident molecules are to a large extent accommodated to the surface before being re-emitted with kinetic energies corresponding to the surface temperature. From $\sigma_t = 0.9$ it follows that relatively little specular reflection takes

place. Naturally, it should be kept in mind that the values quoted above are only indicative and in reality variations may occur depending on surface temperatures, velocities and angles of incidence as well as material properties of the surface.

The pressures and shearing stresses appearing in equations (1) and (2) can be determined from the classical Maxwell distribution function by integrating over all possible values of the velocity space as shown, for instance, by Koppenwallner [6]

$$p_i = \rho v_m^2 \beta f(\beta)/(2\sqrt{\pi}) \tag{3}$$

$$p_w = \rho v_m^2 \sqrt{(T_w/T)}\, g(\beta)/4 \tag{4}$$

$$\tau_i = \rho v_m^2 \beta g(\beta) \tan\theta/(2\sqrt{\pi}) \tag{5}$$

where v_m is the most probable thermal speed of incident molecules, T is the atmospheric temperature, and ρ is the air density, and the following abbreviations have been used

$$f(\beta) = \exp(-\beta^2) + \sqrt{\pi}\,[\beta + 1/(2\beta)]\{1 + \operatorname{erf}(\beta)\} \tag{6}$$

$$g(\beta) = \exp(-\beta^2) + \sqrt{\pi}\,\{1 + \operatorname{erf}(\beta)\} \tag{7}$$

$$\beta = (v/v_m)\cos\theta \tag{8}$$

$$\operatorname{erf}(\beta) = 2/\sqrt{\pi} \int_0^\beta \exp(-x^2)\,dx \tag{9}$$

The angle of incidence θ of the flow with respect to the normal of a surface element is shown in Fig. 1. For the range of ambient atmospheric temperatures between 500 and 1500 °K the *molecular speed ratio* v/v_m would be between about 16 and 11 for typical perigee speeds (10.2 km/s). This means that the expected thermal speeds of the molecules are small in comparison to the orbital velocity.

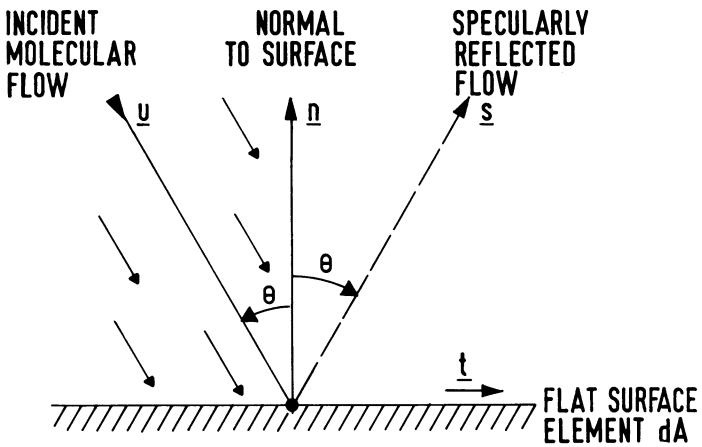

FIG. 1. Flat Surface Element in Uniform Free-Molecular Flow.

The pressure and shear stress induced by the flow follow directly from equations (1) and (2)

$$p = p_i + p_r = (2 - \sigma_n)p_i + \sigma_n p_w \tag{10}$$

$$\tau = \tau_i - \tau_r = \sigma_t \tau_i \tag{11}$$

The direction of the pressure p acts opposite to $\mathbf{n}$ in Fig. 1 and that of the shearing stress acts in a positive direction with respect to the incident flow, i.e. along unit-vector $\mathbf{t}$. Substitution of the expressions of equations (3)-(5) into equations (10) and (11) gives

$$p = \rho v_m^2\{(2 - \sigma_n)\beta f(\beta)/(2\sqrt{\pi}) + \sigma_n\sqrt{(T_w/T)}\, g(\beta)/4\} \tag{12}$$

$$\tau = \rho v_m^2 \sigma_t \beta g(\beta) \tan\theta/(2\sqrt{\pi}) \tag{13}$$

These results contain two free parameters, i.e. the accommodation coefficients σ_n and σ_t which are essentially determined by the surface conditions.

Special Model for Geostationary Transfer Orbits

In the case of typical (ARIANE) Geostationary Transfer Orbits (GTO) a few simplifications can be performed which would make the model presented above more tractable for routine applications. Since the molecular speed ratio is expected to be above 11 as noted before the following inequalities are valid

$$\exp(-\beta^2) < 0.003\beta\sqrt{\pi}\{1 + \operatorname{erf}(\beta)\}, \qquad \beta > 2 \tag{14}$$

$$|\operatorname{erf}(\beta) - 1| < 0.003, \qquad \beta > 2 \tag{15}$$

Therefore, $\operatorname{erf}(\beta)$ may be replaced by 1 and the term $\exp(-\beta^2)$ can be neglected altogether for all value of β larger than 2. The functions f and g defined in equations (6) and (7) become now

$$f(\beta) \cong 2\sqrt{\pi}\,[\beta + 1/(2\beta)], \qquad \beta > 2 \tag{16}$$

$$g(\beta) \cong 2\beta\sqrt{\pi}, \qquad \beta > 2 \tag{17}$$

For still larger values of β a further approximation can be made

$$f(\beta) \cong g(\beta) \cong 2\beta\sqrt{\pi}, \qquad \beta > 7 \tag{18}$$

which holds true with less than one percent error. Remembering the definition of β in equation (8) it is seen that the approximation of equations (16) and (17) can be applied regardless of atmospheric temperature as long as the angle of incidence θ is less than 77 degrees. The stronger approximation in equation (18) holds when θ is less than 37 degrees. For a typical ARIANE GTO the angle of incidence at perigee for the directly exposed surface area would be about 20°, so that equation (18) could be used. For the side walls the angle of incidence is around 70° so that equations (16) and (17) can still be applied. With the aid of the expressions obtained in equations (16) and (17) the following simplified formulas for the normalized pressure and shear stresses can be established

$$p^* = p/(\rho v^2/2) = (2 - \sigma_n)[2\cos^2\theta + (v_m/v)^2] + \sigma_n\sqrt{\pi}\,(v_w/v)\cos\theta \tag{19}$$

$$\tau^* = \tau/(\rho v^2/2) = \sigma_t \sin(2\theta) \tag{20}$$

These results are visualized in Fig. 2 for a representative value of $T_w/T = 0.3$ and $\sigma_n = 1.0$, $\sigma_t = 0.9$. It is seen that even for rather extreme values of v/v_m the behavior of the pressure p^* does not change significantly. Therefore, it appears that the knowledge of v_m (or the ambient atmospheric temperature T) is not very critical for arriving at acceptable torque results.

From the expressions in equations (19) and (20) the drag and lift coefficients which represent the resulting forces (per unit area) in the direction opposite to the velocity vector and normal to it, respectively, can be obtained immediately

$$C_D(\theta) = \rho^* \cos\theta + \tau^* \sin\theta \tag{21}$$

$$C_L(\theta) = \rho^* \sin\theta - \tau^* \cos\theta \tag{22}$$

For the parameters used in Fig. 2 the maximum value of the lift coefficient is near $\theta = 30°$ but amounts to only about 6 percent of that of the drag coefficient (for θ near 5°).

Torque on Arbitrarily Oriented Spinning Surface Element

General Geometry

The torque acting on an arbitrarily oriented spinning surface element will be derived from the expressions for the normal and shear force coefficients as given in

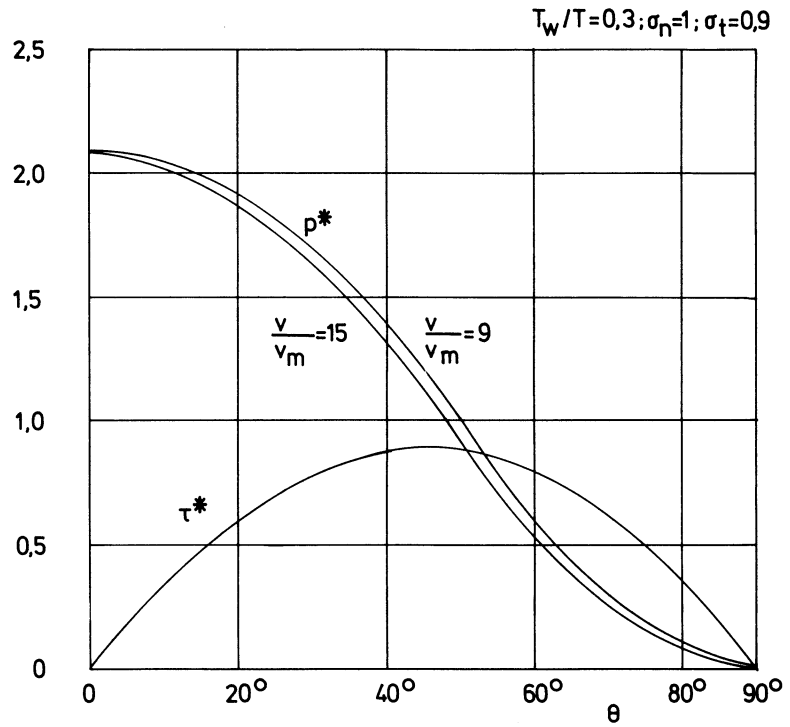

FIG. 2. Normalized Pressure p^* and Shear Stress τ^* as Function of Angle of Incidence θ.

equations (19) and (20). It is evident that the torque depends on the orientation of the orbital velocity vector relative to the body-fixed reference frame which contains the surface element. In terms of components along the local reference frame with unit-vectors $\boldsymbol{\xi}$, $\boldsymbol{\eta}$, $\boldsymbol{\zeta}$ (Fig. 3) the orbital velocity vector can be expressed in the form

$$\mathbf{v} = \dot{r}\boldsymbol{\xi} + (h/r)\boldsymbol{\eta} = (\mu/h)\{e \sin \nu\, \boldsymbol{\xi} + (1 + e \cos \nu)\boldsymbol{\eta}\} \tag{23}$$

The orbital radius is r, the eccentricity and true anomaly are e and ν, and the orbital angular momentum (per unit mass) is h. μ is the Earth's gravitational parameter. The transformation matrix between the local $\boldsymbol{\xi}$, $\boldsymbol{\eta}$, $\boldsymbol{\zeta}$ and inertial **X**, **Y**, **Z** reference frames is well known

$$\begin{bmatrix} \boldsymbol{\xi} \\ \boldsymbol{\eta} \\ \boldsymbol{\zeta} \end{bmatrix} = \begin{bmatrix} \cos \tilde{\nu} \cos \Omega - \sin \tilde{\nu} \sin \Omega \cos i & \cos \tilde{\nu} \sin \Omega + \sin \tilde{\nu} \cos \Omega \cos i & \sin \tilde{\nu} \sin i \\ -\sin \tilde{\nu} \cos \Omega - \cos \tilde{\nu} \sin \Omega \cos i & -\sin \tilde{\nu} \sin \Omega + \cos \tilde{\nu} \cos \Omega \cos i & \cos \tilde{\nu} \sin i \\ \sin \Omega \sin i & -\cos \Omega \sin i & \cos i \end{bmatrix} \begin{bmatrix} \mathbf{X} \\ \mathbf{Y} \\ \mathbf{Z} \end{bmatrix} \tag{24}$$

The argument of latitude $\tilde{\nu}$ is $\nu + \omega$, where ν is true anomaly and ω is the argument of perigee, as indicated in Fig. 3. The right ascension and inclination are Ω and i. By virtue of equations (23) and (24) the velocity vector **v** can be expressed in terms of the components along the inertial **X**, **Y**, **Z** axes.

The satellite's spin axis attitude vector **z** is usually identified by its right ascension α and declination δ in inertial space

$$\mathbf{z} = (\cos \alpha \cos \delta, \sin \alpha \cos \delta, \sin \delta) \begin{bmatrix} \mathbf{X} \\ \mathbf{Y} \\ \mathbf{Z} \end{bmatrix} \tag{25}$$

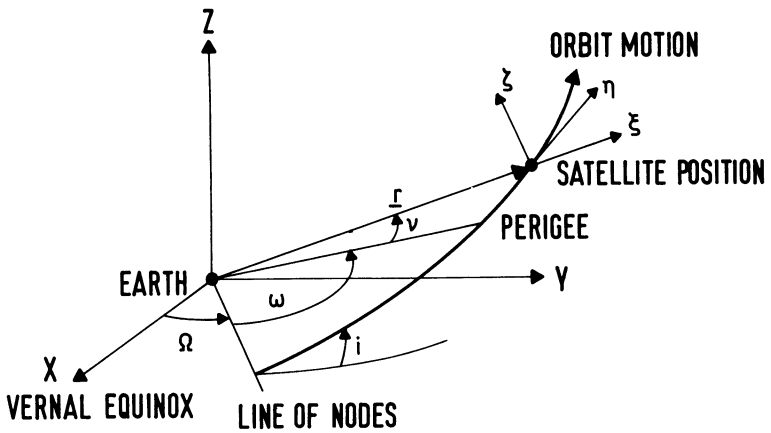

FIG. 3. Geometry of Local ξ, η, ζ Reference Frame.

The angle between **v** and **z** is designated by λ

$$\lambda = \arccos\{[(v_1 \cos \alpha + v_2 \sin \alpha) \cos \delta + v_3 \sin \delta]/v\} \tag{26}$$

The body-fixed satellite frame (**x**, **y**, **z** axes) rotates about the **z** axis with angular rate **w**. In order to simplify subsequent calculations a 'frozen' reference frame ($\mathbf{x}_0$, $\mathbf{y}_0$, $\mathbf{z}_0$ axes) is introduced in such a manner that the velocity vector **v** lies in the $\mathbf{x}_0$, $\mathbf{z}_0$ plane, as indicated in Fig. 4. This frame may be considered quasi-inertial, as it is considered inertially fixed over a certain interval of time until the velocity vector has changed by a prescribed small amount, after which a new frozen frame is established. In most applications it is justified to apply Newton's laws over periods amounting to a number of spin revolutions. The actual body-fixed **x**, **y**, **z** frame follows after rotation over the spin angle $\phi = w(t - t_0)$ with t_0 an epoch where both frames coincide

$$\begin{bmatrix} \mathbf{x} \\ \mathbf{y} \\ \mathbf{z} \end{bmatrix} = \begin{bmatrix} \cos \phi & \sin \phi & 0 \\ -\sin \phi & \cos \phi & 0 \\ 0 & 0 & 1 \end{bmatrix} \begin{bmatrix} \mathbf{x}_0 \\ \mathbf{y}_0 \\ \mathbf{z}_0 \end{bmatrix} \tag{27}$$

Free-Molecular Force on Arbitrary Surface Element

An arbitrarily oriented flat surface element dA with geometrical center at **R** in the body-fixed **x**, **y**, **z** coordinate frame which has its origin at the center of mass is considered in Fig. 5. With the aid of equations (19) and (20) the drag force acting on dA can be expressed in the form

$$d\mathbf{F} = -\frac{1}{2}\rho v^2\{[c_0 + c_1 \cos \theta + c_2 \cos^2 \theta]\mathbf{n} - c_3 \sin \theta \cos \theta \, \mathbf{t}\} dA \tag{28}$$

with

$$c_0 = (2 - \sigma_n)(v_m/v)^2 \tag{29}$$

$$c_1 = \sigma_n(v_m/v)(\pi T_w/T)^{1/2} = \sigma_n\sqrt{\pi}\,(v_w/v) \tag{30}$$

$$c_2 = 2(2 - \sigma_n) \tag{31}$$

$$c_3 = 2\sigma_t \tag{32}$$

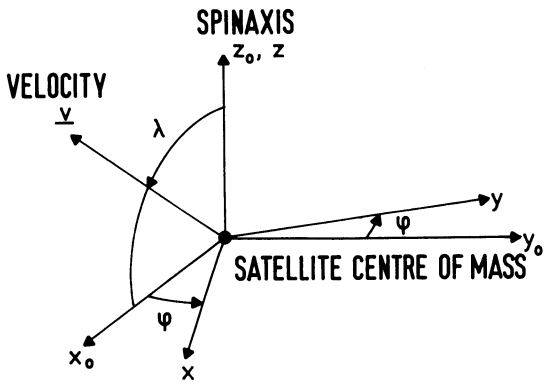

FIG. 4. Geometry of Quasi-Inertial Frozen Frame x_0, y_0, z_0 and Body-Fixed Frame x, y, z.

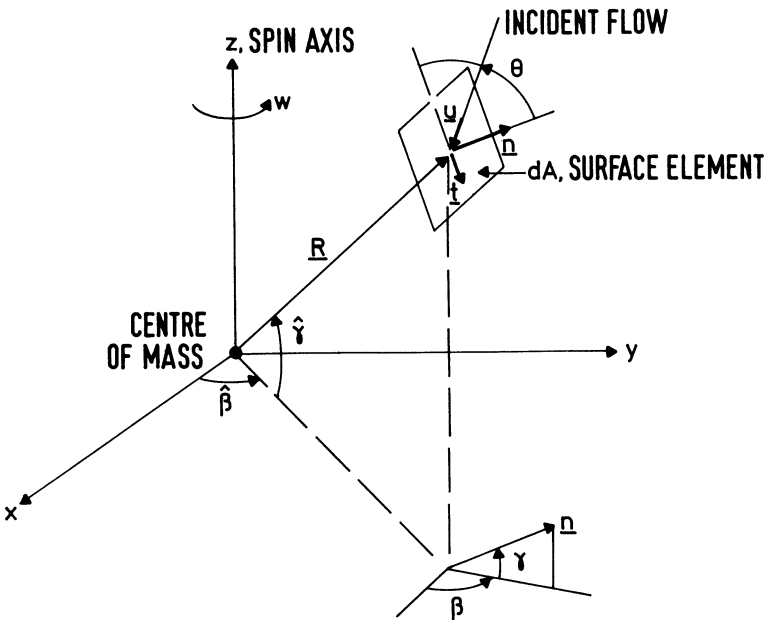

FIG. 5. Orientation of Flat Surface Element in Body-Fixed Frame.

The unit-vectors **n** and **t** refer to the outward normal to the surface and the tangential direction on the surface pointing away from the incident flow, as shown in Fig. 1

$$\mathbf{u} = \sin\theta\,\mathbf{t} - \cos\theta\,\mathbf{n} \tag{33}$$

It turns out to be advantageous to write the force vector in terms of **u** and **n** rather than in **t** and **n**

$$d\mathbf{F} = -\frac{1}{2}\rho v^2\{[c_0 + c_1\cos\theta + (c_2 - c_3)\cos^2\theta]\mathbf{n} - c_3\cos\theta\,\mathbf{u}\}\,dA \tag{34}$$

The coefficients c_j $(j = 0, \ldots, 3)$ can be interpreted physically as follows: c_0 is the normal momentum transfer of incident and specularly reflected molecules due to thermal speed, c_1 is the normal momentum transfer of molecules re-emitted after accommodation at surface temperature, c_2 is the normal momentum transfer of incident and specularly reflected molecules due to orbital speed, and c_3 is the transverse momentum transfer of incident molecules which are not specularly reflected.

In the derivation of equation (34) a simplification has been imposed, namely the velocity of the spinning surface element is taken equal to the satellite's velocity vector. This means that the rotational velocity wR has been neglected in comparison to the orbital speed v. This assumption is justified since for the applications at hand dissipative torques produced by the rotational velocity (cf. Beletskii [8]) are indeed essentially smaller than the torques studied here.

Averaged Torque Due to Force Acting on Arbitrary Surface Element

The elementary surface element dA is completely identified by the lever arm $\mathbf{R}$ indicating the position of its geometrical center with respect to the satellite's center of mass and its outward normal vector $\mathbf{n}$. It is convenient to define these vectors in terms of the familiar right ascension and declination angles relative to the body-fixed reference frame as indicated in Fig. 5. Because of the simple relation between the $\mathbf{x}$, $\mathbf{y}$, $\mathbf{z}$ and $\mathbf{x}_0$, $\mathbf{y}_0$, $\mathbf{z}_0$ frames (Fig. 4), it is easy to express $\mathbf{R}$ and $\mathbf{n}$ in terms of the quasi-inertial frozen frame, using the orientation angles indicated in Fig. 5

$$\mathbf{R} = R\{\cos(\phi + \hat{\beta}) \cos \hat{\gamma}\, \mathbf{x}_0 + \sin(\phi + \hat{\beta}) \cos \hat{\gamma}\, \mathbf{y}_0 + \sin \hat{\gamma}\, \mathbf{z}_0\} \tag{35}$$

$$\mathbf{n} = \cos(\phi + \beta) \cos \gamma\, \mathbf{x}_0 + \sin(\phi + \beta) \cos \gamma\, \mathbf{y}_0 + \sin \gamma\, \mathbf{z}_0 \tag{36}$$

The drag force acts only when $(\mathbf{u} \cdot \mathbf{n}) < 0$, which amounts to the interval bounded by the limiting values ϕ_1, ϕ_2 found by solution of the following equation

$$\mathbf{u} \cdot \mathbf{n} = -\sin \lambda \cos \gamma \cos(\phi + \beta) - \cos \lambda \sin \gamma = 0 \tag{37}$$

The two solutions can be expressed as

$$\phi_{1,2} = -\beta \pm \chi \tag{38}$$

where

$$\chi = \arccos(-\tan \gamma / \tan \lambda) \tag{39}$$

The resulting intervals over which the drag force is acting can be visualized from Fig. 6 for the relevant square in the λ, γ plane. The following eight cases may be distinguished.

Case I $(0 < \lambda < \pi/2,\ \lambda < \gamma < \pi/2)$

In this region the argument of the arccos function in equation (39) is always less than -1 so that χ is undetermined. Since for $\phi = -\beta$ one finds $\mathbf{u} \cdot \mathbf{n} = -\sin(\lambda + \gamma) < 0$, it follows that the drag force acts over the full spin period, i.e. $\phi_2 = \phi_1 + 2\pi$.

Case II $(0 < \lambda < \pi/2,\ 0 < \gamma < \lambda)$

Here, the argument $-\tan \gamma / \tan \lambda$ takes values in the range $(-1, 0)$, so that $\pi/2 < \chi < \pi$ with the point $\phi = -\beta$ being within the drag interval.

Case III $(\pi/2 < \lambda < \pi,\ 0 < \gamma < \pi - \lambda)$

Here the argument lies between 0 and 1, so $0 < \chi < \pi/2$ with again $\phi = -\beta$ within the drag interval.

Case IV $(\pi/2 < \lambda < \pi,\ \pi - \lambda < \gamma < \pi/2)$

Here, the argument is larger than 1 and χ is undetermined. At $\phi = -\beta$ one finds $-\sin(\lambda + \gamma) > 0$ for $\pi < \lambda + \gamma < 3\pi/2$, so the drag force is absent over the full spin period, i.e. $\chi = 0$.

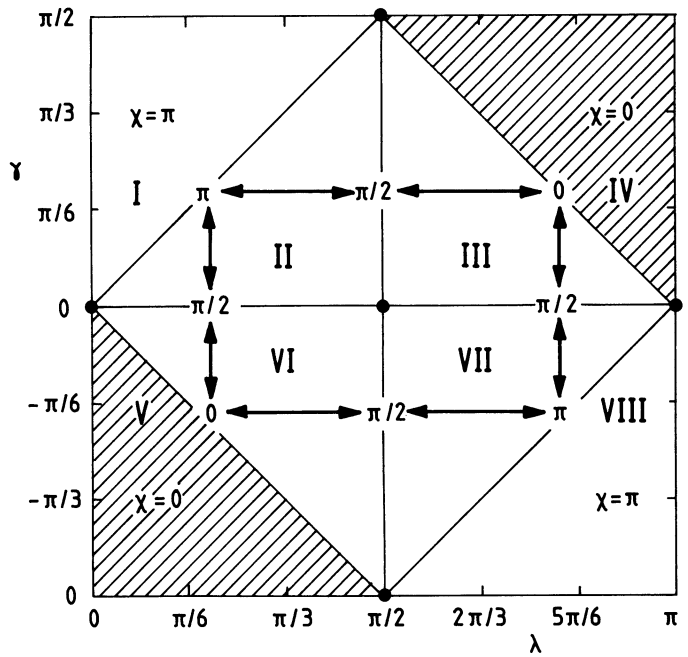

FIG. 6. Visualization of χ as Function of Relevant Values of γ and λ.

The remaining four areas V to VIII in the λ, γ plane can be analyzed in a similar manner. From physical considerations, however, it is evident that complete symmetry exists between (λ, γ) and $(\pi - \lambda, -\gamma)$, as is seen in Fig. 6.

The torque $d\mathbf{M}$ due to the force $d\mathbf{F}$ acting on a surface element dA follows from equations (34) and (35)

$$d\mathbf{M} = \mathbf{R} \times d\mathbf{F} = -\frac{1}{2}\rho v^2\{[c_0 - c_1(\mathbf{u}\cdot\mathbf{n}) + (c_2 - c_3)(\mathbf{u}\cdot\mathbf{n})^2](\mathbf{R}\times\mathbf{n}) + c_3(\mathbf{u}\cdot\mathbf{n})(\mathbf{R}\times\mathbf{u})\}dA \tag{40}$$

where $\cos\theta = -(\mathbf{u}\cdot\mathbf{n})$ has been substituted. After averaging this torque over the interval where the drag force acts, i.e. (ϕ_1, ϕ_2), the following representation is established

$$(d\mathbf{M})_{average} = -\frac{1}{2}\rho v^2\{c_0\mathbf{N}_0 - c_1\mathbf{N}_1 + (c_2 - c_3)\mathbf{N}_2 + c_3\mathbf{U}\}dA \tag{41}$$

with

$$\mathbf{N}_j = 1/(2\pi)\int_{\phi_1}^{\phi_2}(\mathbf{u}\cdot\mathbf{n})^j(\mathbf{R}\times\mathbf{n})\,d\phi, \qquad j = 0, 1, 2 \tag{42}$$

$$\mathbf{U} = 1/(2\pi)\int_{\phi_1}^{\phi_2}(\mathbf{u}\cdot\mathbf{n})(\mathbf{R}\times\mathbf{u})\,d\phi \tag{43}$$

In order to evaluate these integrals, the angular variable $\psi = \phi + \beta$ corresponding to the phase of $\mathbf{n}$ relative to the quasi-inertial $\mathbf{x}_0$, $\mathbf{y}_0$, $\mathbf{z}_0$ frame is introduced. With the aid of the expressions in equations (35) and (36) it can be seen that

$$\mathbf{u} \cdot \mathbf{n} = B_0 + B_1 \cos \psi \tag{44}$$

$$\mathbf{R} \times \mathbf{n} = R\{(C_1 \cos \psi + C_2 \sin \psi)\mathbf{x}_0 + (C_1 \sin \psi - C_2 \cos \psi)\mathbf{y}_0 - C_3\mathbf{z}_0\} \tag{45}$$

$$\mathbf{R} \times \mathbf{u} = R\{(D_1 \cos \psi - D_2 \sin \psi)\mathbf{x}_0 + (D_0 + D_1 \sin \psi + D_2 \cos \psi)\mathbf{y}_0 + (D_3 \cos \psi + D_4 \sin \psi)\mathbf{z}_0\} \tag{46}$$

with coefficients

$$B_0 = -\sin \gamma \cos \lambda \tag{47}$$

$$B_1 = -\cos \gamma \sin \lambda \tag{48}$$

$$C_1 = \cos \hat{\gamma} \sin \gamma \sin(\hat{\beta} - \beta) \tag{49}$$

$$C_2 = \cos \hat{\gamma} \sin \gamma \cos(\hat{\beta} - \beta) - \sin \hat{\gamma} \cos \gamma \tag{50}$$

$$C_3 = \cos \hat{\gamma} \cos \gamma \sin(\hat{\beta} - \beta) \tag{51}$$

$$D_0 = -\sin \hat{\gamma} \sin \lambda \tag{52}$$

$$D_1 = -\cos \hat{\gamma} \cos \lambda \sin(\hat{\beta} - \beta) \tag{53}$$

$$D_2 = \cos \hat{\gamma} \cos \lambda \cos(\hat{\beta} - \beta) \tag{54}$$

$$D_3 = \cos \hat{\gamma} \sin \lambda \sin(\hat{\beta} - \beta) \tag{55}$$

$$D_4 = \cos \hat{\gamma} \sin \lambda \cos(\hat{\beta} - \beta) \tag{56}$$

Since all of the angles appearing here are fixed with respect to the satellite frame (cf. Fig. 5) all coefficients B_j, C_j and D_j are constants. When substituting the results of equations (44)–(46) into the integrals in equations (42) and (43), four non-vanishing integrals $I_j, j = 0, \ldots, 3$ can be identified in which each of $\mathbf{N}_j$ and $\mathbf{U}$ can be expressed

$$I_j = 1/(2\pi) \int_{\psi_1}^{\psi_2} (\cos \psi)^j d\psi, \qquad j = 0, 1, 2, 3 \tag{57}$$

Due to the symmetry of the integration interval relative to $\psi = 0$, all integrals containing an odd power of $\sin \psi$ vanish. The integrals in equation (57) have been evaluated for the different regions displayed in Fig. 6, as shown in Table 1. It is seen that continuity is preserved across the borders of no-drag and full drag regions.

The integrals $\mathbf{N}_j$ and $\mathbf{U}$ defined in equations (42) and (43) can now be expressed in terms of $I_j, j = 0, \ldots, 3$ using the results of equations (44)-(46)

$$\mathbf{N}_0 = R\{C_1 I_1 \mathbf{x}_0 - C_2 I_1 \mathbf{y}_0 - C_3 I_0 \mathbf{z}_0\} \tag{58}$$

$$\mathbf{N}_1 = R\{(B_0 I_1 + B_1 I_2)(C_1 \mathbf{x}_0 - C_2 \mathbf{y}_0) - C_3(B_0 I_0 + B_1 I_1)\mathbf{z}_0\} \tag{59}$$

$$\mathbf{N}_2 = R\{(B_0^2 I_1 + 2B_0 B_1 I_2 + B_1^2 I_3)(C_1 \mathbf{x}_0 - C_2 \mathbf{y}_0) - C_3(B_0^2 + 2B_0 B_1 I_1 + B_1^2 I_2)\mathbf{z}_0\} \tag{60}$$

TABLE 1. Summary of Integrals I_j for Different Regions in (λ, γ) Plane (cf. Fig. 6)

Regions	ψ_1	ψ_2	I_0	I_1	I_2	I_3
I, VIII	$-\pi$	π	1	0	1/2	0
II, VII, III, VI	$-\chi$	χ	χ/π	$(\sin\chi)/\pi$	$(\chi + \sin\chi\cos\chi)/2\pi$	$(\sin\chi)/\pi - (\sin^3\chi)/3\pi$
IV, V	0	0	0	0	0	0

$$\mathbf{U} = R\{(B_0 I_1 + B_1 I_2)(D_1\mathbf{x}_0 + D_2\mathbf{y}_0 + D_3\mathbf{z}_0) + D_0(B_0 I_0 + B_1 I_1)\mathbf{y}_0\} \quad (61)$$

The general result given in equations (41) and (58)–(61) completes the calculation of the averaged torque acting on a flat arbitrarily oriented spinning surface element dA. It should be noted that the result is expressed in terms of components along the frozen reference frame. The axes belonging to this frame are allowed to slowly vary from one spin revolution to the next.

Torque on Idealized Satellite Configurations

Cylindrical Shell

The analysis presented above for an elementary surface element dA is now extended to an actual surface configuration, i.e. a cylindrical shell representing the surface of a spinning rotationally symmetric spacecraft (Fig. 7). The result of equation (41) with averaged integrals given in equations (58)–(61) refers to the torque contribution of a single surface element dA averaged over a complete spin revolution. By integration

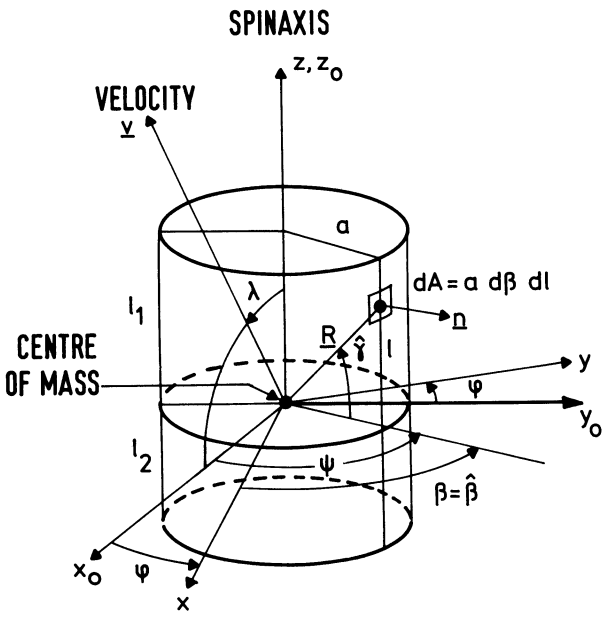

FIG. 7. Geometry of a Cylindrical Satellite Configuration.

over the full surface area, the total resulting torque acting on the satellites is obtained. With the aid of cylindrical shell coordinates β, ℓ (so that $dA = a\,d\beta\,d\ell$, where a is the cylindrical shell radius and $0 \leq \beta \leq 2\pi$, $-\ell_2 \leq \ell \leq \ell_1$) the averaged total torque can be expressed as

$$\mathbf{M}_{average} = -\frac{1}{2}\rho v^2 a \int_{\beta=0}^{2\pi} \int_{\ell=-\ell_2}^{\ell_1} \{c_0\mathbf{N}_0 - c_1\mathbf{N}_1 + (c_2 - c_3)\mathbf{N}_2 + c_3\mathbf{U}\}\,d\beta\,d\ell \tag{62}$$

For a particular cylindrical surface element one has $\beta = \hat{\beta}$, so $\mathbf{n} = \cos\beta\mathbf{x} + \sin\beta\mathbf{y}$ with $\gamma = 0$ and $\mathbf{R} = a(\cos\beta\mathbf{x} + \sin\beta\mathbf{y}) + \ell\mathbf{z}$ with $\hat{\gamma} = \arctan(\ell/a)$. This means that the coefficients in equations (47)–(56) can be simplified to

$$B_0 = C_1 = C_3 = D_1 = D_3 = 0 \tag{63}$$

$$B_1 = -\sin\lambda \tag{64}$$

$$C_2 = -\ell/R \tag{65}$$

$$D_0 = -(\ell/R)\sin\lambda \tag{66}$$

$$D_2 = (a/R)\cos\lambda \tag{67}$$

$$D_4 = (a/R)\sin\lambda \tag{68}$$

Substitution of these coefficients in the vector integrals of equations (58)–(61) leads to

$$\mathbf{N}_0 = \ell I_1\,\mathbf{y}_0 \tag{69}$$

$$\mathbf{N}_1 = -\ell I_2 \sin\lambda\,\mathbf{y}_0 \tag{70}$$

$$\mathbf{N}_2 = \ell I_3 \sin^2\lambda\,\mathbf{y}_0 \tag{71}$$

$$\mathbf{U} = (\ell I_1 \sin\lambda - aI_2\cos\lambda)\sin\lambda\,\mathbf{y}_0 \tag{72}$$

The integrals I_j, $j = 1, 2, 3$ are determined by the fact that $\chi = \pi/2$ as can be seen from Fig. 6 for $\gamma = 0$ and any value of λ. Table 1 provides now the results

$$I_1 = 1/\pi \tag{73}$$

$$I_2 = 1/4 \tag{74}$$

$$I_3 = 2/(3\pi) \tag{75}$$

With these results the final torque expression can readily be established by integration of equation (62) over the cylinder

$$\mathbf{M}_{average} = -\frac{1}{2}\rho v^2 a(\ell_1 + \ell_2)\left\{(\ell_1 - \ell_2)\left[c_0 + c_1(\pi/4)\sin\lambda + \frac{1}{3}(2c_2 + c_3)\sin^2\lambda\right] - ac_3(\pi/4)\sin(2\lambda)\right\}\mathbf{y}_0 \tag{76}$$

The validity of this result has been confirmed by a comparison with an exact formula provided by Gustafson [9]; the difference is due to terms of order $(v_m/v)^2$ in the coefficient of $\sin^2 \lambda$ and amounts to less than 1 percent for the molecular speed ratios considered here.

It is of interest to note that the resulting torque vector acts along $\mathbf{y}_0$, i.e. in a direction normal to the plane defined by the spin and velocity vectors. This qualitative result can be confirmed by symmetry considerations.

Circular Flat Surface Area

An actual cylindrical satellite configuration is also affected by the drag force acting on one of its flat circular sides. In terms of polar coordinates s, β one has $dA = s\,ds\,d\beta$ and

$$\mathbf{M}_{average} = -\frac{1}{2}\rho v^2 \int_{\beta=0}^{2\pi} \int_{s=0}^{a} \{c_0\mathbf{N}_0 - c_1\mathbf{N}_1 + (c_2 - c_3)\mathbf{N}_2 + c_3\mathbf{U}\} s\,ds\,d\beta \tag{77}$$

Since $\mathbf{n} = \pm\mathbf{z}$ and $\mathbf{R} = s(\cos\beta\,\mathbf{x} + \sin\beta\,\mathbf{y}) \pm R_c\mathbf{z}$ the corresponding right ascension and declination angles become $\beta = \hat{\beta}$, $\gamma = \pm\pi/2$, and $\hat{\gamma} = \pm\arctan(R_c/s)$, where R_c designates the distance from the centre of the surface to the centre of mass. The $+$, $-$ sign refers to a top and bottom surface, respectively.

The coefficients appearing in the vector integrals can be simplified as follows

$$B_0 = \mp\cos\lambda \tag{78}$$

$$B_1 = C_1 = C_3 = D_1 = D_3 = 0 \tag{79}$$

$$C_2 = \pm s/R \tag{80}$$

$$D_0 = \mp(R_c/R)\sin\lambda \tag{81}$$

$$D_2 = (s/R)\cos\lambda \tag{82}$$

$$D_4 = (s/R)\sin\lambda \tag{83}$$

From Fig. 6 it is seen that the drag force acts only for $0 < \lambda < \pi/2$ in the case $\gamma = \pi/2$ and for $\pi/2 < \lambda \leq \pi$ when $\gamma = -\pi/2$. In both of these cases the drag acts over the full interval. According to Table 1 the integrals I_j become under these conditions

$$I_0 = 1 \tag{84}$$

$$I_1 = I_3 = 0 \tag{85}$$

$$I_2 = 1/2 \tag{86}$$

The resulting averaged torque over the circular surface area can now be evaluated using the expressions in equations (58)–(61) and integrating as indicated in equation (77)

$$\mathbf{M}_{average} = -\frac{1}{4}\rho v^2 A R_c c_3 \sin(2\lambda)\mathbf{y}_0 \tag{87}$$

with $A = \pi a^2$. The resulting torque acts along the negative $\mathbf{y}_0$ direction when it is a "top" surface (i.e., $\gamma = \pi/2$ and $0 < \lambda < \pi/2$) and along the positive $\mathbf{y}_0$ direction when it is a "bottom" surface (i.e., $\gamma = -\pi/2$ and $\pi/2 < \lambda < \pi$). The torque found here is due to the incident transverse momentum transfer of molecules which are not specularly reflected.

Rectangular Flat Surface Area

The general results are now applied to an extended flat surface with area A rotating about the satellite's spin axis and oriented arbitrarily with respect to the satellite's equatorial plane. The orientation is indicated by the angles β and γ designating the right ascension and declination of the outward normal to the surface within the spacecraft frame, cf. Fig. 5. The position vector of the geometric centre of the surface with respect to the centre of mass is denoted by $\mathbf{R}_c$.

It is helpful to recognize that the shape of the rectangular surface area does not enter into the final torque results (as long as the surface characteristics such as temperatures and accommodation coefficients can be considered to be homogeneous, of course). This can be understood on the basis of symmetry considerations: the contributions of a certain surface element dA at $\mathbf{R} = \mathbf{R}_c + \boldsymbol{\rho}$ can be split up in a "main" part due to $\mathbf{R}_c$ and a "relative" part due to $\boldsymbol{\rho}$. The latter contribution is cancelled by the corresponding contribution of the "opposite" element at $\mathbf{R}' = \mathbf{R}_c - \boldsymbol{\rho}$ as can readily be seen from the integrals in equations (42) and (43). Therefore, the integration of the vector functions $\mathbf{N}_j$, $j = 0, 1, 2$ and $\mathbf{U}$ over the surface area A can be performed immediately

$$\mathbf{M}_{average} = -\frac{1}{2}\rho v^2 A\{c_0\mathbf{N}_0 - c_1\mathbf{N}_1 + (c_2 - c_3)\mathbf{N}_2 + c_3\mathbf{U}\}_{\mathbf{R}=\mathbf{R}_c} \tag{88}$$

with applicable expressions for the integrals $\mathbf{N}_j$ and $\mathbf{U}$ given in equations (58)-(61) for the general case.

While the results obtained are valid for an arbitrary surface orientation, the explicit expression of the torque vector components in all relevant angles becomes rather unwieldy. Therefore, a more practical special case is considered in some detail.

A flat "side-surface" area with centre at $\mathbf{R}_c$ from the centre of mass is considered. The normal $\mathbf{n}$ to the surface is oriented such that its right ascension β is equal to $\hat{\beta}$ in the spacecraft frame, cf. Figs. 5 and 8. Note also that $\gamma = 0$ so that $\chi = \pi/2$ as is seen in Fig. 6, whereas the declination of $\mathbf{R}_c$ is

$$\hat{\gamma} = \arctan\{R_z/(R_x^2 + R_y^2)^{1/2}\} \tag{89}$$

The relevant coefficients in equations (47)–(56) can now be written as

$$B_0 = C_1 = C_3 = D_1 = D_3 = 0 \tag{90}$$

$$B_1 = -\sin\lambda \tag{91}$$

$$C_2 = -\sin\hat{\gamma} \tag{92}$$

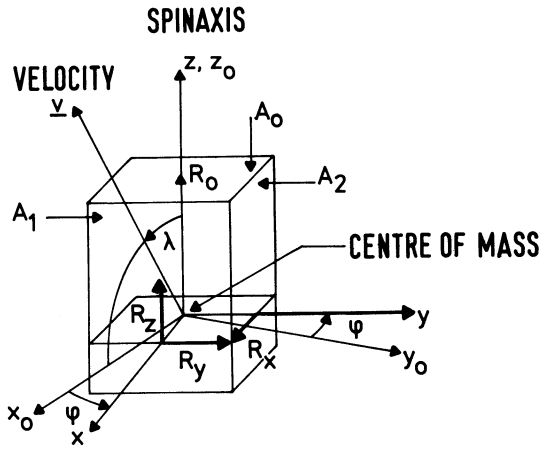

FIG. 8. Geometry of a Box-Like Satellite Configuration.

$$D_0 = -\sin\hat{\gamma}\sin\lambda \tag{93}$$

$$D_2 = \cos\hat{\gamma}\cos\lambda \tag{94}$$

$$D_4 = \cos\hat{\gamma}\sin\lambda \tag{95}$$

On the basis of equations (58)–(61) and (88), and the results of Table 1 for $\chi = \pi/2$, as given in equations (73)–(75), the total torque can be written as

$$\mathbf{M}_{average} = -\rho v^2 A R_c/(2\pi)\left\{\sin\hat{\gamma}\left[c_0 + c_1(\pi/4)\sin\lambda + \frac{1}{3}(2c_2 + c_3)\sin^2\lambda\right] - c_3(\pi/8)\cos\hat{\gamma}\sin(2\lambda)\right\}\mathbf{y}_0 \tag{96}$$

It may be mentioned that a torque component along the $\mathbf{x}_0$ or $\mathbf{z}_0$ direction can only arise if $\beta \neq \hat{\beta}$, cf. equations (47)–(56) and (58)–(61). In this case the projection of $\mathbf{R}_c$ and $\mathbf{n}$ of a given surface area into the satellite's equatorial plane would not be aligned.

Finally, it may be noted that in the case of a rectangular top or bottom surface the same result as in equation (87) for a circular area can be reestablished.

Regular Box-Like Configuration

The results established above are useful in establishing the total torque acting on a regular box-like satellite as shown in Fig. 8. The side-surfaces have pairwise equal areas A_1 and A_2 with the four centers $\mathbf{R}_1\pm = (\pm R_x, 0, R_z)$ and $\mathbf{R}_2\pm = (0, \pm R_y, R_z)$, respectively. In the case when $\lambda < \pi/2$ a torque will also be generated by the top surface with area A_0 and center $\mathbf{R}_0 = (0, 0, R_0)$. If $\lambda > \pi/2$ the bottom surface with $\mathbf{R}_0 = (0, 0, -R_0)$ will have a contribution. Note that R_x, R_y and R_0 are defined as positive distances, but R_z will be negative when the center of mass would lie above the geometric centers of the sidesurfaces, cf. Fig. 8. The corresponding declinations of the five relevant surfaces are

$$\gamma_0 = \pm\pi/2 \qquad (\text{for } \lambda \lesseqgtr \pi/2) \tag{97}$$

$$\gamma_1^{\pm} = \arctan(R_z/R_x) \tag{98}$$

$$\gamma_2^{\pm} = \arctan(R_z/R_y) \tag{99}$$

By adding the contributions of the four surface areas pairwise using equation (96) as well as that of the top or bottom surface as given in equation (87), the total torque can readily be established

$$\mathbf{M}_{average} = -\rho v^2 \left\{ (A_1 + A_2)(R_z/\pi) \left[c_0 + c_1(\pi/4) \sin\lambda + \frac{1}{3}(2c_2 + c_3) \sin^2\lambda \right] - \frac{1}{8}(A_1 R_x + A_2 R_y - 2A_0 R_0) c_3 \sin(2\lambda) \right\} \mathbf{y}_0 \tag{100}$$

The sign of $\pi/2 - \lambda$ defines whether R_0 designates the distance to the top or bottom surface area.

Concluding Remarks

An approximate model for free-molecular flow effects on a satellite surface area has been developed. The model is particularly aimed at applications related to spinning satellites in geostationary transfer orbit with perigee altitude near 200 km. The resulting torque on an arbitrarily oriented surface area has been established by first integrating the contribution of an infinitesimal surface element over the relevant part of one spin revolution. Subsequently, an integration over the total surface area is performed. The expressions obtained should be useful for calculating the torque expressions of fairly elaborate spacecraft structures. Results are given in explicit form for two simple geometrical satellite configurations of cylindrical and box-like shapes.

The formulation reported here was recently applied in an analysis of actually observed attitude variations of the MARECS-A satellite during its three perigee passages in geostationary transfer orbit, cf. Van der Ha [7].

References

[1] SCHAAF, S. A. and CHAMBRÉ, P. L. *Flow of Rarefied Gases,* Princeton University Press, 1961.

[2] COOK, G. E. "Satellite Drag Coefficients," *Planetary Space Sciences,* Vol. 13, 1965, pp. 929–946.

[3] IZAKOV, M. N. "Allowance for a Variable Aerodynamic Drag Coefficient in Deriving the Air Density from Satellite Decelerations," *Cosmic Research,* Vol. 3, 1965, pp. 211–220.

[4] BOETTCHER, R. D. "The Calculation of Convex Body Aerodynamics in Free Molecular Flow using a Plane Element Surface Approximation," *ESA CR(X) 1278,* Part I, 1979.

[5] BOETTCHER, R. D. and LEGGE, H. "Determination of Aerodynamic Forces on Satellites by Theory and Wind Tunnel Experiments," *Acta Astronautica,* Vol. 7, 1980, pp. 255–267.

[6] KOPPENWALLNER, G. "Freimolekulare Aerodynamik für Satellitenanwendung," *DFVLR Forschungsbericht,* 82–08, 1982.

[7] VAN DER HA, J. C. "Attitude Perturbations Induced by Free-Molecular Flow Interactions in Perigee Region," IAF-85-232, Stockholm, Sweden, October 1985, *Acta Astronautica,* Vol. 13, 1986, pp. 301–309.

[8] BELETSKII, V. V. "Motion of Artificial Satellite about its Centre of Mass," NASA TT F-429, 1966.

[9] GUSTAFSON, W. A. "Aerodynamic Moment on Bodies Moving at High Speed in the Upper Atmosphere," *ARS Journal,* Vol. 29, No. 4, April 1959.